Journal of Hydroscience and Hydraulic Engineering
Vol. 8, No. 2, December, 1990, 21-37

CALCULATION OF BOUNDARY SHEAR STRESS IN OPEN CHANNEL FLOW

by

Kouji Houjou
Hokkaido Development Agency, Tokyo, Japan,

Yasuyuki Shimizu
Civil Engineering Research Institute, Sapporo, Japan

and

Chimataro Ishii
Akita University, Akita, Japan

SYNOPSIS

This paper presents a method for calculating the velocity field in open channel flows for which lateral shear is an important factor. It is based on the assumption of a scalar eddy viscosity that is proportional to the shear velocity on the actual flow boundary at the base of any isovel-normal-ray and the area up to the isovel of interest between two adjacent rays divided by their separation distance at the boundary. The momentum equation produced by this turbulence closure is solved numerically. In a channel with a rectangular cross section, the flow structure depends on both the width-depth ratio and the wall-bed roughness ratio. For such channels figures to evaluate the boundary shear stress distribution on the bed are provided. The validity of the model is tested using the experimental data obtained by Imamoto and Ishigaki(1988). The utility of the model, when applied to sediment transporting flows, is demonstrated using William's (1970) experimental data, which cover a wide range of width-depth ratios and wall-bed roughness ratios.

INTRODUCTION

Quantitative information concerning lateral variations in mean velocity and turbulence properties is necessary for understanding the boundary shear stress and sediment transport fields in natural and artificial flow systems, because all such systems have lateral boundaries (e.g. banks or side walls) on which some of the fluid work is dissipated. For problems related to bank erosion and channel migration, an accurate knowledge of the boundary shear stress distribution is required in order to permit precise computation of the divergence of the sediment transport rate. Reliable estimates of velocities and boundary shear stresses in near bank regions are essential for designing bank protection works and other hydraulic structures. Moreover, in flume studies, the effects of side walls must be calculated and removed especially in relatively narrow channels with a low ratio of bed to side wall roughness.

Most of the previous research on boundary shear stress distributions in natural and artificial channels has focused on the bed shear stress because this provides a good approximation to that in the central region of channels of relatively large width-depth ratio. Einstein (1942) proposed a method for taking into account the wall effect in rectangular channels, assuming that the mean velocities in the areas affected by the walls and those affected by the bed were equal to the cross sectionally averaged velocity; this is not physically correct. Consequently, Williams (1970), as part of a comprehensive bed load transport investigation, developed an empirical equation to evaluate the effective bed shear stress in flumes with vertical side walls. William's equation

includes the depth-width ratio, but does not explicitly account for the wall-bed roughness ratio, and therefore, it can not be applied to situations other than flumes with smooth walls in which sediment is being transported as bed load and the bedforms are in equilibrium with the hydraulic regime. Also it gives only the cross sectional averaged value of the boundary shear stress, and thus it is impossible to estimate the boundary shear stress distributions along the bed or over the walls. Work on boundary shear stress distribution in straight channels was also carried out by Lundgren and Jonsson (1964). Their pioneering analytical study has served as a foundation for recent work on this topic and on bank erosion. Their theory, however, is only valid for systems with relatively small lateral slopes. The aim of the present paper is to extend their methods to channels with vertical walls.

In this paper, which is concerned with flumes, lined channels and irrigation ditches rather than natural rivers, streamwise variations in velocity will be neglected so that the two-dimensional (depth and width) momentum equation can be solved to determine the complete velocity and shear stress structure in a cross section. The scalar eddy viscosity is calculated along rays, which are everywhere perpendicular to the isovels. Calculations are performed for a wide range of width-depth ratios as well as for a number of wall-bed roughness ratios. In each case, the calculated boundary shear stresses are compared with those obtained from the depth-slope product. Graphs that permit evaluation of the ratio of actual boundary shear stress to that computed using the depth-slope product are presented as a function of the width-depth and wall-bed roughness ratios. The calculation is verified using the experimental data obtained by Imamoto and Ishigaki(1988), and the utility of the model is provided using William's(1970) experimental data on sediment transport in channels of various width-depth ratios. In the calculation for William's(1970) experiment, the pressure drag associated with bedforms is removed so that bed load transport rates are computed properly. This is done using the method of Smith and McLean (1977) as modified by Wiberg and Smith (1989).

FLOW IN A STRAIGHT CHANNEL WITH INFINITE WIDTH

In order to lay a strong quantitative foundation for the lateral stress problem, the flow field without lateral friction is described in this section; this is, in essence, the flow in a channel of infinite width. The momentum equation for steady and horizontally uniform flow in a straight channel is

$$-\rho g S = \frac{\partial \tau_{zx}}{\partial z} = \frac{\partial}{\partial z}\left(\rho K \frac{\partial u}{\partial z}\right) \tag{1}$$

where g is the acceleration due to gravity, S is the downstream surface slope of stream, ρ is the density of the fluid, τ_{zx} is the component of deviatoric stress in the downstream direction on a surface parallel to the channel bed, u is the velocity component in the downstream direction, K is a kinematic eddy viscosity, x is the down-stream coordinate and z is the coordinate normal to bed. Integrating Eq. 1 with respect to z, and using the boundary condition that $\partial u/\partial z = 0$ and $\tau_{zx} = 0$ at the water surface, gives,

$$\tau_{zx} = \rho K \frac{\partial u}{\partial z} = \rho g S D \left(1 - \frac{z}{D}\right) \tag{2}$$

As $\tau_{zx} = \tau_0$ at $z = 0$, the bed shear stress is $\tau_0 = \rho g S D$, and

$$\tau_{zx} = \tau_0 \left(1 - \frac{z}{D}\right) \tag{3}$$

Using the shear velocity $u_* = \sqrt{\tau_0/\rho}$ this becomes

$$\tau_{zx} = \rho K \frac{\partial u}{\partial z} = \rho {u_*}^2 \left(1 - \frac{z}{D}\right) \tag{4}$$

where D is water depth. As can be seen, the boundary shear stress here is proportional to the depth-slope product. Eq. 3 yields a linear shear stress profile. The eddy viscosity can be described for an infinitely wide channel flow using the approximation of Rattray and Mitsuda (1974);

$$\begin{aligned} K &= ku_*z\left(1-\frac{z}{D}\right) && \frac{z}{D} < 0.2 \\ K &= ku_*\frac{D}{\beta} && \frac{z}{D} \geq 0.2 \end{aligned} \tag{5}$$

where k is Von Karman's constant and β is 6.24. Eq. 5 reproduces the best fit velocity profile to the Einstein and Chien's (1950) experimental data. Combining Eqs. 4 and 5, then integrating with respect to z with the boundary condition that $u = 0$ at $z = z_{0b}$, yields

$$\begin{aligned} \frac{u}{u_*} &= \frac{1}{k}\ln\frac{\xi}{\xi_0} && \xi < 0.2 \\ \frac{u}{u_*} &= \frac{1}{k}\left[\ln\frac{0.2}{\xi_0} + \beta\left(\xi - 0.5\xi^2 - 0.18\right)\right] && \xi \geq 0.2 \end{aligned} \tag{6}$$

where $\xi = z/D$, $\xi_0 = Z_{0B}/D$ and Z_{0B} = roughness height at the channel bed. The vertically averaged velocity $< u >$ is obtained by integrating Eq. 6 from $z = 0$ to $z = D$, then dividing by D. This gives

$$\frac{< u >}{u_*} = \frac{1}{k}\left(\ln\frac{D}{\xi_0} - 0.745\right) \tag{7}$$

The discharge per unit width is $q =< u > D$, and the net discharge for a very wide flow in a rectangular channel is approximated by $Q =< u > DW$ where W is the channel width, the error being of order D/W.

In an unaccelerated flow, bed plus wall friction must balance the downstream component of the gravitational force. So the shear stress averaged over the wetted perimeter of the channel must equal

$$(\tau_0)_{AV} = \rho g S\frac{A}{p} \tag{8}$$

where A is the cross sectional area of the flow, p is the wetted perimeter and A/p is hydraulic radius. Sometimes $(\tau_0)_{AV}$ is used as an estimate of the stress on the channel bottom, especially in sediment transport studies. Typically it yields an underestimation of the boundary shear stress in those parts of the channel where the sediment transport rates are highest. In contrast, $\tau = \rho g S D$ usually overestimates the boundary shear stress in these regions. As $W \rightarrow \infty$, $A/p \rightarrow D$ and these estimates merge.

FLOW WITH LATERAL BOUNDARIES

The lefthand side of Eq. 1 arises from the divergence of the deviatoric stress tensor, and a second term is required to express this force per unit volume in a fully two-dimensional flow. For an unaccelerated flow in which a scalar eddy viscosity closure is appropriate, the proper momentum equation is

$$-\rho g S = \frac{\partial}{\partial z}\left(K\frac{\partial u}{\partial z}\right) + \frac{\partial}{\partial n}\left(K\frac{\partial u}{\partial n}\right) \tag{9}$$

where n is the transverse coordinate. For an infinitely wide flow, the Rattray and Mitsuda eddy viscosity of Eq. 5 depends only on the z coordinate, but in the fully two dimensional case, it is also a function of n. In fact, the mixing processes act across surfaces of constant velocity in the direction of the shear, and the appropriate length scale for these eddies must be calculated along lines (rays) which are perpendicular to the isovels (velocity contour lines) as shown in Fig. 1(a).

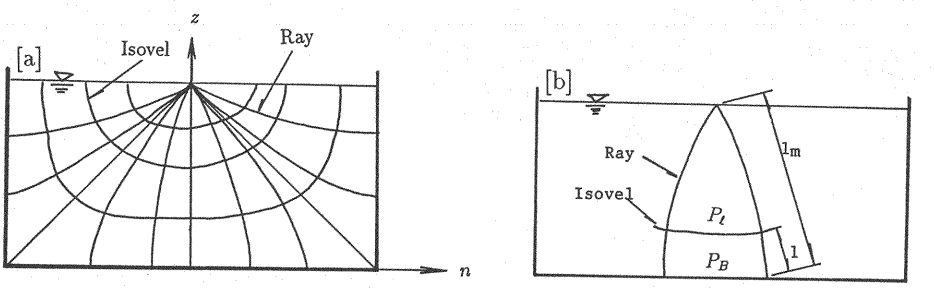

Fig. 1 Description sketch of isovels (contours of the downstream velocity) and their orthogonals, which are denoted rays in this paper. (b)Notations for Eq. 11.

The eddy viscosity, therefore, can be a function only of the shapes of the rays and the shear stress at their intersections with the boundary. The profile of eddy viscosity must collapse to that of Eq. 5, when the rays become parallel to each other, but in general the length scale of the turbulence depends on the geometry of the rays and is not simply the distance along the ray from the boundary. Rather it is an area weighted function of the distance from the boundary. Therefore, we write;

$$K = ku_*\ell\gamma \tag{10}$$

where ℓ is the distance from the boundary along the ray and γ is an area weighted function of ℓ. In an infinitely wide flow γ must collapse to $(1 - z/D) = (D - z)/D$ as required by Eq. 5. The form of γ is thus chosen to be;

$$\gamma = \frac{\dfrac{\int_\ell^{\ell_m} dA}{P_\ell}}{\dfrac{\int_0^{\ell_m} dA}{P_B}} \tag{11}$$

where ℓ_m is the length of the ray, P_ℓ is the perimeter along the isovel and P_B is the perimeter along the boundary [see Fig.1(b)]. When the rays become parallel the numerator of Eq. 11 reduces to $(D - z)$ and the denominator reduces to D. In the calculations, the constant value is employed when two-tenths of area between rays in achieved, so

$$\begin{aligned} K &= ku_*\ell\gamma \qquad && \int_0^{\ell} dA < 0.2\int_0^{\ell_m} dA \\ K &= K_0 && \int_0^{\ell} dA \geq 0.2\int_0^{\ell_m} dA \end{aligned} \tag{12}$$

where K_0 is the value of K at $\int_0^{\ell} dA = 0.2 \int_0^{\ell_m} dA$.

For a given surface slope, Eq. 9 can be coupled with Eq. 12 and solved using the boundary condition that $\partial u/\partial z = 0$ at $z = D$ and $u = 0$ at $\ell = \ell_0$, in which ℓ_0 is the roughness length (usually denoted z_0 in the infinitely wide case). Eq. 9 is solved using a finite difference method in an orthogonal (n, z) grid, while Eq. 12 is calculated in a ray-isovel grid. Shear velocity u_* in Eq. 12 is calculated from,

$$\rho u_*^2 = \tau_B = \rho K \frac{\partial u}{\partial \ell} \qquad \text{at} \qquad \ell = \ell_0 \tag{13}$$

The locus of the rays are calculated from,

$$\tan\theta = \frac{\dfrac{\partial u}{\partial z}}{\dfrac{\partial u}{\partial n}} \tag{14}$$

in which, θ is the angle of the rays from a horizontal line. Eqs. 9 and 12 are solved alternately until a constant solution is obtained.

Depth averaged velocities and discharges are calculated numerically from the solutions of Eq. 9. Owing to the complexity of the system, the velocity and eddy viscosity fields and the discharge of the flow can not be calculated with sufficient accuracy using an analytical approach, as for the situation when Eq. 12 collapses to Eq. 5.

Table 1: Conditions for the calculation of rectangular channels and calculated value of R_*

Fig. No.	D(cm)	W(cm)	W/D	Z_{0B}(cm)	Z_{0W}(cm)	Z_{0B}/Z_{0W}	R_*
2	10.0	20.0	2.0	0.001	0.001	1.0	0.50
3	5.0	40.0	8.0	0.001	0.001	1.0	0.84
4	15.0	15.0	1.0	0.001	0.001	1.0	0.27
5	10.0	20.0	2.0	0.01	0.001	10.0	0.62
6	10.0	20.0	2.0	0.001	0.01	0.1	0.36

CALCULATED RESULTS IN RECTANGULAR CHANNEL

Fig. 2 shows results calculated from Eq. 9 for a channel with a rectangular cross section. The four panels of Fig. 2, from the bottom up, show (a)rays, (b)isovels, (c)velocities, with the solid line being the depth-averaged velocity and the dashed line being the surface velocity, and (d)the cross sectional distribution of the ratio of bottom shear stress to that obtained from the depth-slope product. The conditions for the calculation are summarized in Table 1 together with the conditions for Figs. 3, 4, 5 and 6, which will be described in this section. Here z_{0W} and z_{0B} are the values of ℓ_0 at the side walls and on the channel bed respectively, and R_* is the the cross sectionally averaged value of the ratio of bed shear stress to the shear stress obtained from the depth-slope product, that is;

$$R_* = \frac{1}{W} \int_{-W/2}^{W/2} \frac{\tau_B}{\tau_0} dn \tag{15}$$

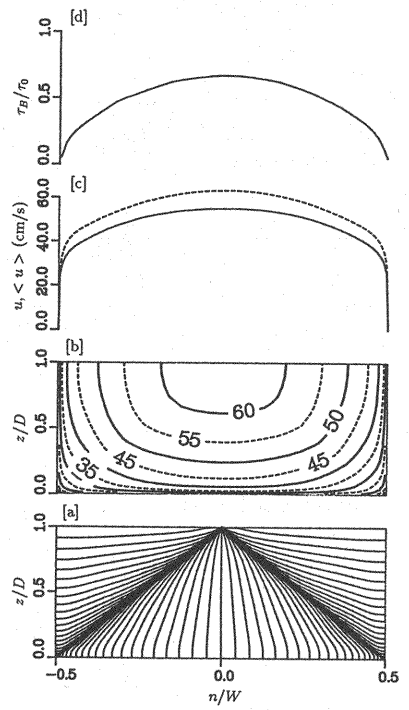

Fig. 2 Calculated results for a channel of rectangular cross section: (a)rays, (b)isovels, (c)depth-averaged velocity (solid line) and surface velocity (dashed line), and (d)ratio of calculated boundary shear stress to that obtained from the depth-slope product.

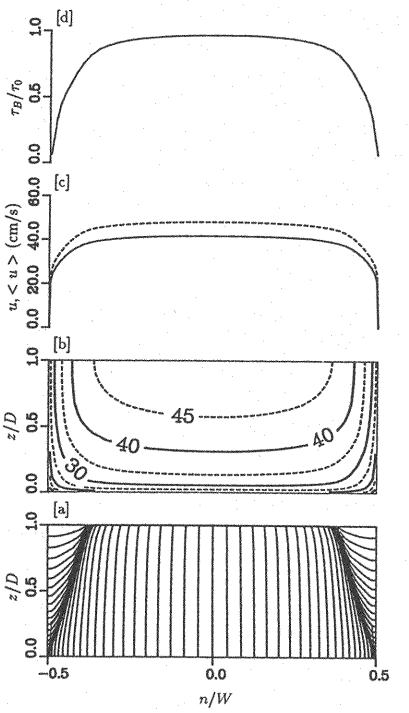

Fig. 3 Calculated results for a channel of rectangular cross section: (a)rays, (b)isovels, (c)depth-averaged velocity (solid line) and surface velocity (dashed line), and (d)ratio of calculated boundary shear stress to that obtained from the depth-slope product.

In this case, since the roughnesses of walls and bed are the same and the channel shape is half of a square ($W/D = 2$), the velocity profile is symmetrical in the z and n directions. The maximum velocity is in the channel center at the water surface and all of the rays converge at this point. The boundary shear stress at each submerged corner is zero, and there is a large reduction in maximum boundary shear stress compared to that given by the depth-slope product. The average bed shear stress is nearly half ($R_* = 0.5$) of that of depth-slope product.

Fig. 3 shows results of computations for a relatively wide channel ($W/D = 8$), with the roughness of walls and bed again held the same. The order and the description of each of the panels in the figure are the same as those for Fig. 2. In this case, the effects of the walls are limited to the neighborhood of the walls and the rays near the channel center are nearly parallel to each other, which means the velocity profile in this region is almost the same as that given by Eq. 6 for the infinite width case. Depth averaged velocity, surface velocity and boundary shear stress are almost constant except near the walls; moreover, $R_* = 0.841$ which indicates that the wall effect is relatively small in this case.

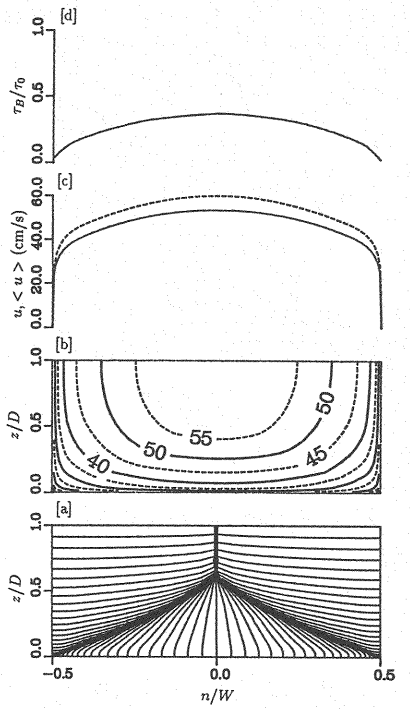

Fig. 4 Calculated results for a channel of rectangular cross section: (a)rays, (b)isovels, (c)depth-averaged velocity (solid line) and surface velocity (dashed line), and (d)ratio of calculated boundary shear stress to that obtained from the depth-slope product.

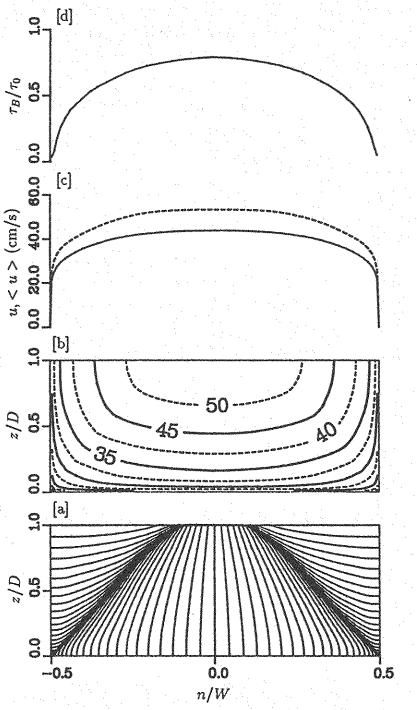

Fig. 5 Calculated results for a channel of rectangular cross section: (a)rays, (b)isovels, (c)depth-averaged velocity (solid line) and surface velocity (dashed line), and (d)ratio of calculated boundary shear stress to that obtained from the depth-slope product.

In contrast, Fig. 4 shows results of a calculation for a relatively narrow channel ($W/D = 1$). The locus of the rays displays large wall effects and the frictional effect of the channel bed is not able to penetrate beyond mid depth. The shear stress on the bed is much smaller than that given by the depth-slope product and the average value of R_* is about 0.30.

Figs. 5 and 6 show the effects of roughness ratio differences. The width-depth ratio for these two cases is the same as that for Fig. 2 ($W/D = 2$), however, the bed is ten times rougher than the walls in Fig. 5 and the walls are ten times rougher than the bed in Fig. 6. The same phenomena are seen here in Figs. 3 and 4, namely, when the bed is rough (Fig. 5), the effect of the bed is large making the wall effect weaker, and when the walls are rough (Fig. 6), the effect of walls are large making the bed effect weaker. Consequently, the averaged boundary shear stress at the bed is much smaller than that of depth-slope product when the walls are rougher, and the wall effect is smaller when the walls are smoother. These results are intuitively obvious because, when the wall is infinitely smooth or the channel is infinitely wide, the effect of walls is eliminated and the flow can be treated neglecting lateral boundary shear stresses. In this cases the boundary shear stress will be identical to that obtained from the depth-slope product.

The boundary shear stress distribution on the bed is often of considerable importance, for example, high near bank boundary shear stresses are of concern in bank erosion problems. Also it is necessary to know the actual shear stress on the channel bed in most flume experiments, especially those conducted for sediment-transport purposes. The theory and computational method described in this paper provide a powerful tool for evaluating boundary shear stress distributions in channels of various roughness distributions and geometries; however, it is not practical to have to carry out calculations using the model for each situation of interest. Also, after doing a series of calculations such as those described above, it was found that the ratio of evaluated boundary shear stress to that given by the depth-slope product depends primarily on (1) the width-

depth ratio and (2) the wall-bed roughness ratio. Consequently calculations using a wide range of width-depth ratios and wall-bed roughness ratios were performed.

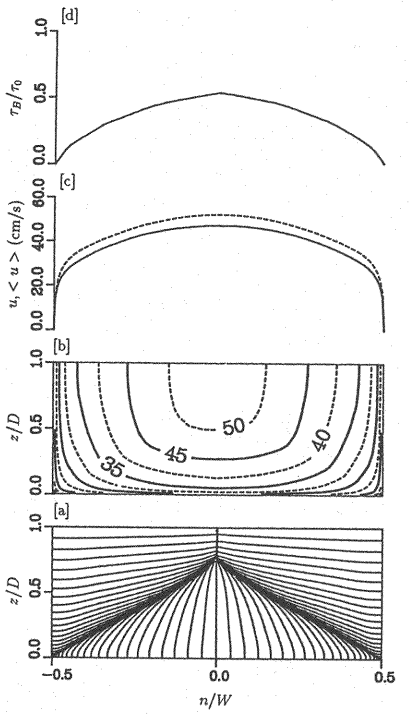

Fig. 6 Calculated results for a channel of rectangular cross section: (a)rays, (b)isovels, (c)depth-averaged velocity (solid line) and surface velocity (dashed line), and (d)ratio of calculated boundary shear stress to that obtained from the depth-slope product.

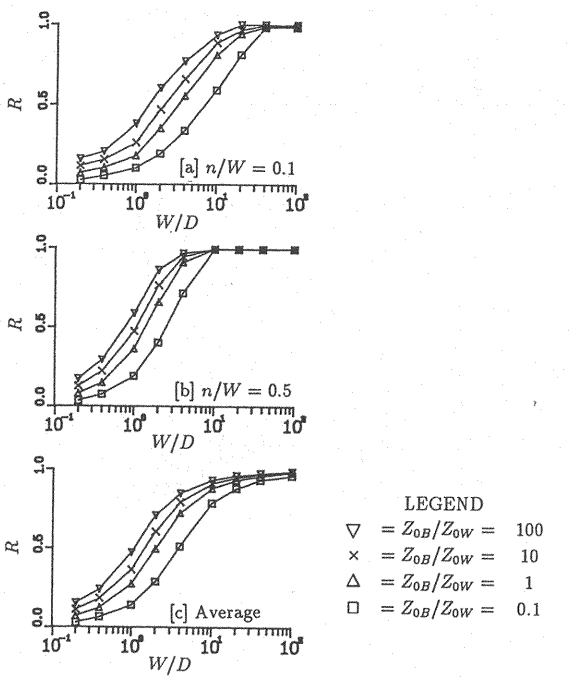

Fig. 7 Distribution of the ratio of calculated boundary shear stress to that obtained from depth-slope product (R) as a function of the width-depth ratio (W/D) and bed-wall roughness ratio Z_{0B}/Z_{0W}, at (a) a near wall region ($n/W = 0.1$), (b) the center of the channel ($n/W = 0.5$), and (c) the cross stream averaged value.

In Fig. 7(a), the vertical axis ($R = \tau_B/\tau_0$), is the ratio of boundary shear stress to that obtained from the depth-slope product at the channel center ($n/W = 0$), while the horizontal axis is the width-depth ratio (W/D) and the different symbols indicate different bed-wall roughness ratios (Z_{0B}/Z_{0W}). When W/D becomes large, R goes to 1, which indicates that the boundary shear stress approaches that given by the depth-slope product and that wall effects are negligible. With a decrease of W/D, R approaches zero, which indicates that the boundary shear stress is reduced relative to that given by the depth-slope product as a consequence of friction on the channel walls. The larger the value of Z_{0B}/Z_{0W} (the rougher the bed), the larger the value of R, which means the smaller the wall effect. Fig. 7(b), for which the description is the same as that for Fig. 7(a), shows the boundary shear stress near the wall ($n/W = \pm 0.4$). The general characteristics of R are essentially the same as those displayed in Fig. 7(a), however, of each value of R tends to be larger because of the reduced effects of the wall. Fig. 7(c) shows the cross- sectional averaged value of R, which is equal to R_* defined by Eq. 13. According to Fig. 7(c), in relatively wide channels as ($W/D > 10$) as is common in natural rivers, the values of R_* are usually greater than 0.9, which means that the bank effects are of little significance except locally, and thus calculations neglecting lateral stresses are sufficiently accurate for most engineering purposes except near cut banks. In situations with W/D less than 10, which is common in experimental and artificial channels, however, the effect of lateral stress is important and the analysis described in this section needs to be employed.

VERIFICATION OF THE THEORY AND THE MODEL

In order to test the theory that is described in the previous section of this paper, it has been applied to the data obtained from the experiment with a straight rectangular glass flume conducted by Imamoto and Ishigaki(1988). The flow data of the experiment Case–1 is summarized in Table 2. A calculation was carried out with the same condition with the experiment. l_0 was calculated using Nikurase's(1933) formula for hydraulically smooth flow, namely,

$$l_0 = \frac{\nu}{9u_{*b}} \tag{16}$$

where ν = viscosity of water, u_{*b} = shear velocity at the boundary. Fig. 8 shows the comparison between the observed and calculated velocity and boundary shear stress distribution. The five panels of Fig. 8 show (a)observed u, (b)calculated u, (c)surface velocity u_s and depth-averaged velocity $< u >$, (d)boundary shear stress along the channel bed and (e) boundary shear stress along the side wall. In Fig. 8(c), filled circles and unfilled circles are the observed $< u >$ and u_s, respectively, and solid line and dashed line are the calculated u_s and $< u >$, respectively. In Figs. 8(d) and 8(e), circles and line denote the observed and calculated boundary shear stress, respectively. All the calculated results are favorably compared with the experimental results. A slight disagreement between calculated and observed values in the boundary shear stress distribution along the wall is recognized, and it seems to be because of the effect of the secondary flow, which has not been taken into account for in the present model.

Table 2: Hydraulic conditions of the experiment Case–1 by Imamoto and Ishigaki(1988).

Discharge	$Q(\ell/\mathrm{s})$	2.055
Depth	$D(\mathrm{cm})$	4.01
Slope	S	1/1442
Width	$W(\mathrm{cm})$	39.0

In order to demonstrate the utility of the model in the analysis of laboratory experiments on flow and sediment transport, it has been applied to the comprehensive data set procured by Williams (1970). In this carefully exececuted study, a large number of sediment transport runs were made in a straight flume with many different width-depth ratios ($0.28 < W/D < 20.5$). Although the side walls of the flume were plexiglas and, consequently, had a nearly constant Z_{0W}, the bed of the experimental facility was covered with sand and varied from flat to rippled or duned. As a result, the wall-bed roughness ratio varied from 20 to 10000. In each experiment, water discharge, slope, depth, sediment discharge , and bed form geometry were measured. The bed material used for the experiments was a fairly uniform sand (d = 1.35mm). Fig. 9 shows the range of W/D and Z_{0B}/Z_{0W} for those experiments, where Z_{0W} was calculated using Eq. 16, replacing ℓ_0 with Z_{0W}.

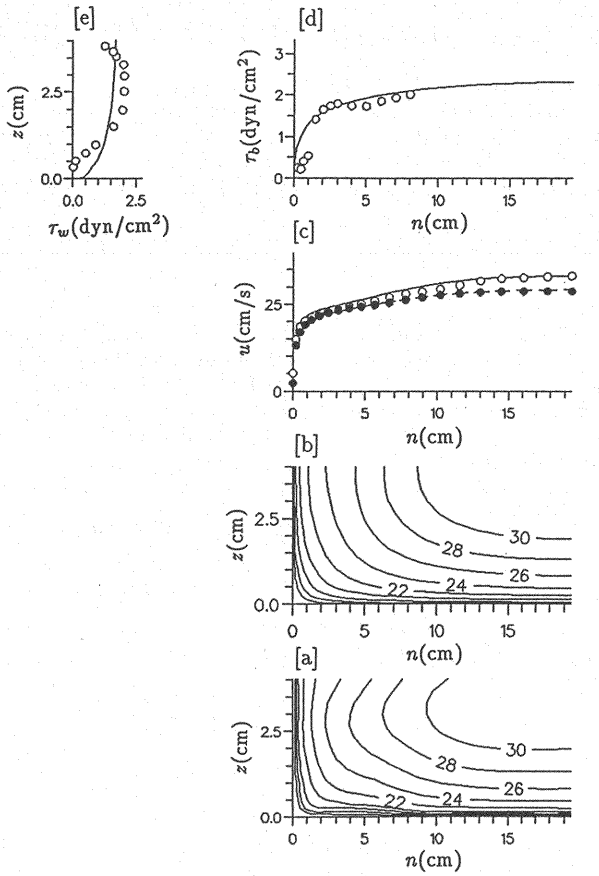

Fig. 8 Comparison of calculated and observed downstream velocity and boundary shear stress distribution: (a)observed u, (b)calculated u, (c)surface velocity u_s and depth-averaged velocity $< u >$, in which filled circles and unfilled circles are the observed $< u >$ and u_s, respectively, and solid line and dashed line are the calculated u_s and observed $< u >$, respectively, (d)boundary shear stress along the channel bed and (e)boundary shear stress along the side wall. In the panel (d) and (e), circles are observed values and lines are the calculated values. Observed values are obtained by Imamoto and Ishigaki(1988).

It is well known that, in the flow over bed forms, the total shear stress (given from the depth-slope product) can be divided into two components (form drag and skin friction) and that sediment transport is associated only with the skin friction. Therefore, a correction must be made to reduce the total stress to skin friction if the sediment transport rates are to be calculated properly. Following Wiberg and Smith (1989), relationship between total stress and the skin friction can be written as

$$\tau_{SF} = \tau_0 \left\{ 1 + \frac{C_D H_B}{2\lambda k^2} \left[\ln \frac{H_B}{(Z_0)_{SF}} - 1 \right]^2 \right\}^{-1} \tag{17}$$

where τ_{SF} is the skin friction, λ is the bed form wavelength, H_B is the bed form height, C_D is the form drag coefficient and $(Z_0)_{SF}$ is the roughness length for the internal boundary layer.

Velocity measurements over large dunes by Smith and McLean (1977) indicate that when separation occurs the drag coefficient C_D is about 0.21. Deitrich (1982) found that $(Z_0)_{SF}$ is proportional to the height of the saltation layer δ_B.

$$(Z_0)_{SF} = 0.08\delta_B \tag{18}$$

Wiberg and Smith (1989) calculated δ_B and for grain size of the William's (1970) experiments, their method yields

$$\frac{\delta_B}{D} = \frac{0.68\frac{\tau_{SF}}{\tau_{CR}}}{1.0 + 0.11\frac{\tau_{SF}}{\tau_{CR}}} \tag{19}$$

where τ_{CR} is the critical shear stress for the initiation of sediment motion. The effective roughness of the channel bed Z_{0B} can be determined by matching the velocity profiles from the internal and outer boundary layers (Nelson and Smith 1989), which yields

$$Z_{0B} = H_B\left[\frac{H_B}{(Z_0)_{SF}}\right]^{-1/\gamma_D}, \qquad \gamma_D = \left[\frac{\tau_{SF} + \tau_0}{\tau_{SF}}\right]^{1/2} \tag{20}$$

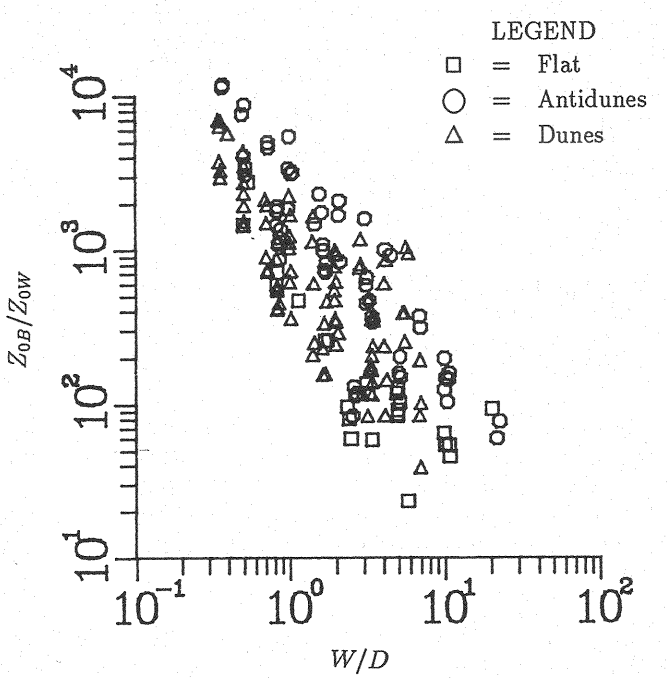

Fig. 9 Range of W/D and Z_{0B}/Z_{0W} in William's (1970) experiments.

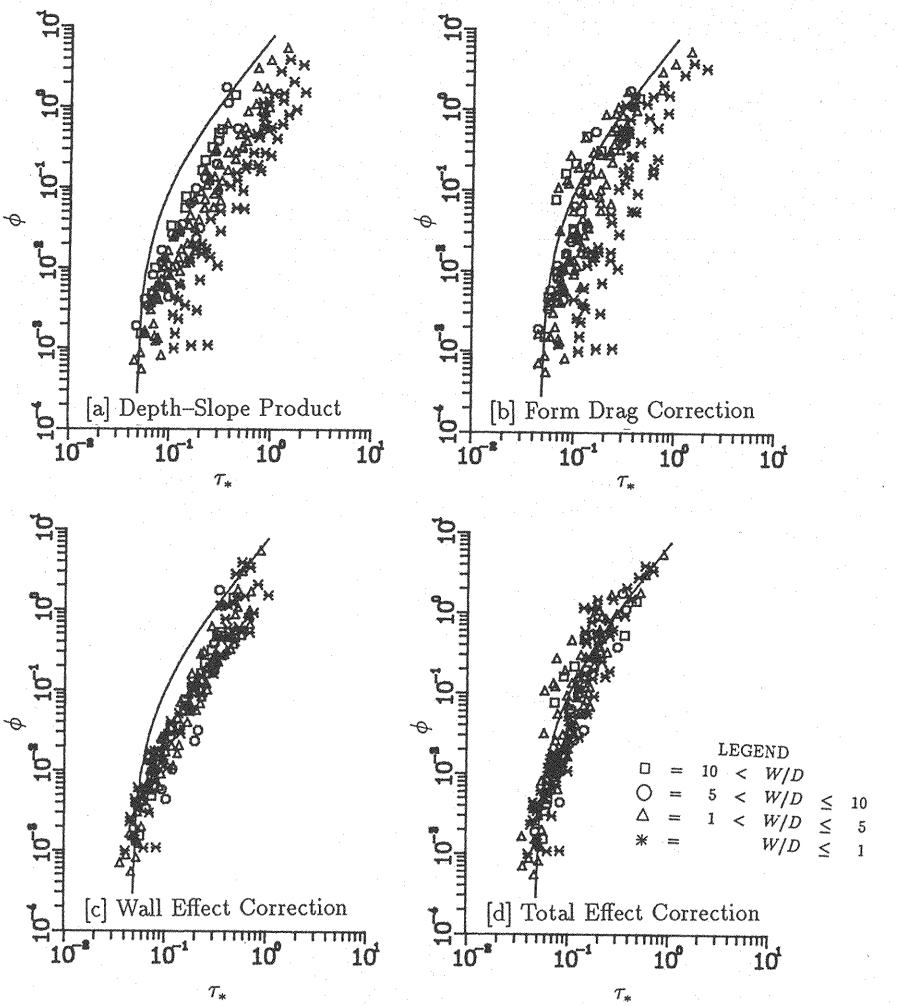

Fig. 10 Williams (1970) data on nondimensional bed load transport, ϕ, as function of nondimensional shear stress compared with Meyer–Peter Muller (1948) equation. In (a) the boundary shear stress is calculated using only the depth-slope product, in (b) a form drag correction has been applied to the depth-slope product based value, in (c) a wall friction correction has been applied to the depth-slope product based value and in (d) both form drag and wall friction correction have been applied.

The nondimensional sediment transport rates calculated using $\phi = q_s/[(\rho_s/\rho - 1)gd^3]^{1/2}$, (where q_s is the sediment discharge per unit width and ρ_s is the density of the bed material) for all of William's(1970) experiments are plotted as a function of nondimensional total stress $\tau_* = \tau_0/[(\rho_s - \rho)gd]$ in Fig. 10(a). Also shown in this figure is the curve obtained from the Meyer–Peter and Muller formula(1948), $\phi = 8(\tau_* - 0.047)^{3/2}$. Most of the measured values fall well to the right of the curve, especially the values associated with small width-depth ratios. Fig. 10(b) shows the same data after the pressure drag associated with the bedforms has been removed from τ_* using Eq.17. This correction shifts the data toward the left because it reduces the effective

value of τ_*. This form drag correction brings the data with large W/D into good agreement with the curves, however, the data with small W/D still fall well to the right of the line because of the wall effect. When a wall correction is made to each of the points of Fig. 10(a) by multiplying the total shear stress by R_*, the results shown in Fig. 10(c) are obtained. This correction matches the points because, as described in the previous section, the narrower the channel, the smaller the effective boundary shear stress due to the wall effect, but the set of points now falls to the right of the line. Only when both corrections are made simultaneous, as in Fig. 10(d), do the data points scatter around the line given by the Meyer–Peter and Muller(1943) formula. Fig. 11 shows the same data as Fig. 10(d), but in this case they are compared with some other common sediment transport formulae. This figure, which is analogues to Fig. 7 of Wiberg and Smith (1989), shows good agreement between the experimental data and common sediment transport expressions.

Sediment transport measurements are often compared with the boundary shear stress obtained using the depth-slope product as shown in Fig. 10(a), and the scattered data tends to be treated as inaccuracy in the sediment transport formula or measurement error. In fact, when τ_* is calculated using the skin friction on the actual sediment bed, good agreement is obtained even in cases for $W/D < 1$, situations which would not ordinarily be considered acceptable for sediment transport studies. The boundary shear stress correction makes the data converge and lead to a favorable comparison with the common sediment transport formulae. From these results, it can be said that neither the experiments nor the formulae were inaccurate, but rather than the most important thing in a sediment transport investigation is how to determine the appropriate boundary shear stress.

The discharge per unit width measured in William's (1970) experiments is compared with calculated values using Eq. 7 in Fig. 12(a) and using the two-dimensional calculation with the lateral stress (Eq. 9) in Fig. 12(b). Calculated values in Fig. 12(a) tend to be over estimates especially for the data with small W/D, which again is because of the wall effect. Better agreement is obtained in Fig. 12(b) because the effects of lateral stress are included in the calculation.

An experimentally determined equation to remove the effect of side wall friction was proposed by Williams (1970). It is;

$$R_* = \frac{1}{1 + 5.5\frac{D}{W^2}} \tag{21}$$

where 5.5 is a constant with dimensions of length measured in centimeters (0.055 in SI units). Fig. 13 shows a comparison between Eq. 21 and calculated values of R_* using the method described above. As the parameter $(W/D)\sqrt{D}$ (horizontal axis of Fig. 13) doesn't include the relative roughness factor of the walls (Z_{0B}/Z_{0W}), the calculated values can not be plotted as a single line, and the scatter of the values in Fig. 13 indicates the effect of relative wall roughness. In general, the calculated values are in good agreement with Eq. 21, but suggest an expression that includes relative wall roughness would yield more accurate results.

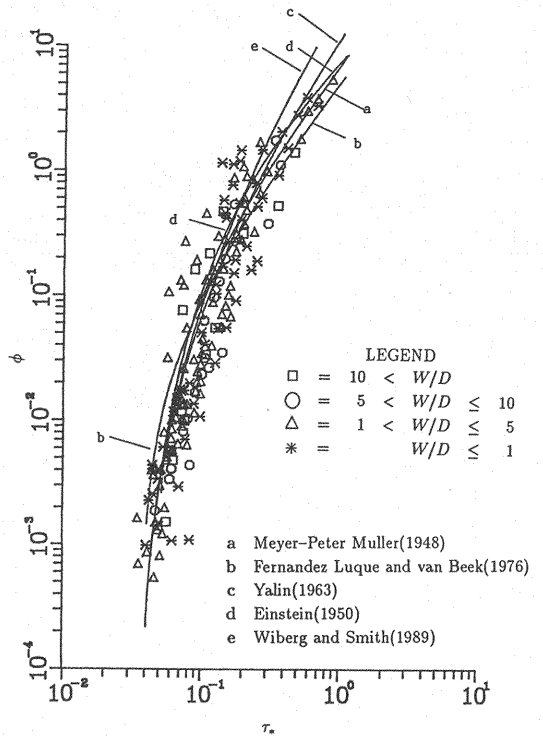

Fig. 11 Nondimensional bed load transport, ϕ, as function of nondimensional shear stress after form drag and wall effect correction are made. The data are compared with formulae proposed by (a) Meyer– Peter Muller(1948), (b) Fernandez Luque and van Beek(1976), (c) Yalin(1963), (d) Einstein(1942) and (e)Wiberg and Smith(1989).

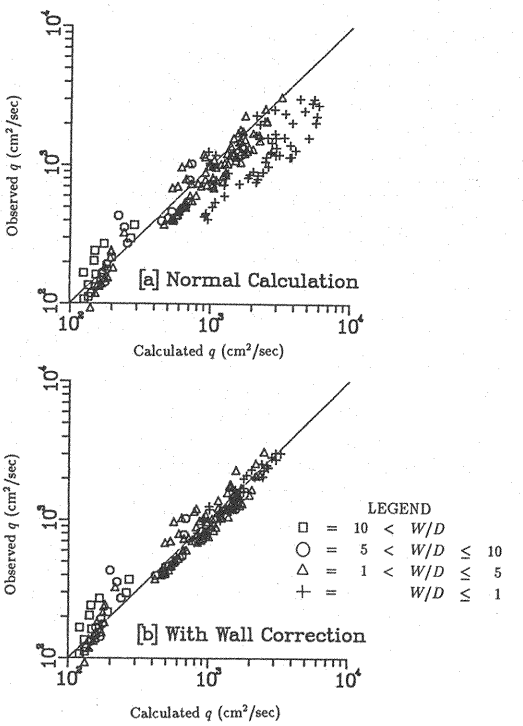

Fig. 12 Comparison of discharge per unit width between observed values and calculated ones by (a) Eq.7 and (b) Eq. 9. The former has wall friction suspended and the latter includes lateral stress.

CONCLUSION

A method to take into account the effects of lateral stress is proposed. It permits computation of velocity and stress fields affected by both the channel bed and channel walls. A two-dimensional momentum equation was solved, coupled with an eddy viscosity calculated along rays perpendicular to the isovels. Characteristics of the flow structure depend only on the width-depth ratio and wall- bed roughness ratio for the case of a uniform flow in a channel of rectangular cross section. Graphs designed to permit the boundary shear stress distribution along the channel bed to be evaluated are proposed. The model was verified using the experimental data obtained by Imamoto and Ishigaki(1988). The utility of the model was demonstrated using William's (1970) experimental data on sediment and water discharge over a wide range of width-depth ratios and wall-bed roughness ratios. The importance of accurate estimation of the boundary shear stress in sediment transport studies is also emphasized by this analysis. Calculated side wall effects agree reasonably well with the empirical formula of William's (1970).

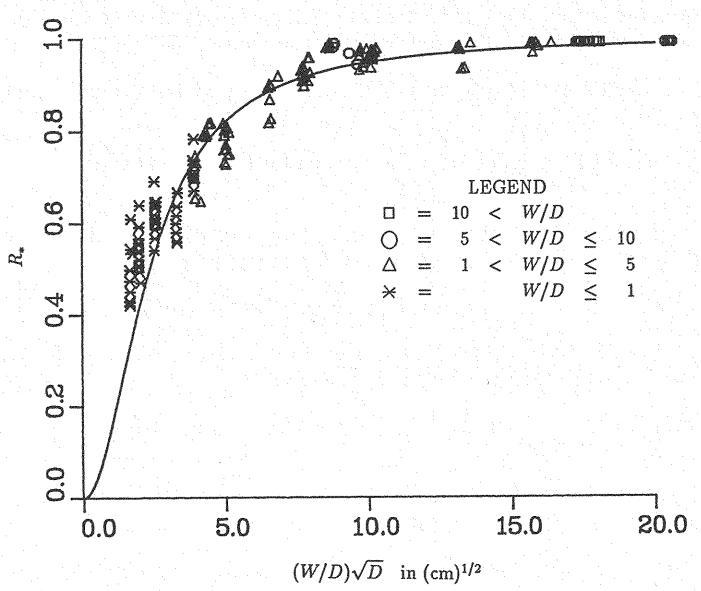

Fig. 13 Distribution of the cross sectional averaged value of the ratio of boundary shear stress to that obtained from the depth-slope product (R_*), as function of $(W/D)D^{0.5}$. The line is from Eq. 21 and symbols are calculated values.

ACKNOWLEDGMENTS

The research described in this paper was completed during the second author's one-year stay in the United States, which was funded through a fellowship program of the Science and Technology Agency of Japanese government. This support is gratefully acknowledged. Also the second author is grateful to U.S. Geological Survey for the use of its facilities and to Professor J. Dungan Smith of the University of Washington for his support and advice during study.

APPENDIX I. – REFERENCES

Deitrich, W. E. (1982). "Flow, boundary shear stress, and sediment transport in a river meander." Ph.D. Dissertation, University of Washington. 1–261.

Einstein, H. A. (1942). "Formulas for the transportation of bed-load." Trans., ASCE, 107, 561–597.

Einstein, H. A. (1950). "The bed load function for sediment transportation in open channel flows." Tech. Bulletin No. 1026, U.S.D.A., Soil Conserv. Service, 1–71.

Einstein, H. A. and Chien, N. (1954). "Second approximation to the solution of the suspended load theory." Fluid Mechanics Laboratory, University of California, Berkeley, 1–12.

Fernandez Luque, R., and van Beek, R. (1976). "Erosion and transport of bed-load sediment." J. Hydr. Res., 14(2), 127–144.

Imamoto, H., and Ishigaki, T. (1988). "Mean and turbulence structure near the inclined side–wall in an open channel flow." Proc. of the 3rd International Symposium on Refined Flow Modeling and Turbulence Measurements, Tokyo, Japan, 545–552.

Lundgren, H., and Jonsson, I. G. (1964). "Shear velocity distribution in shallow channels." J. Hydr. Eng., 90, 1–21.

Meyer–Peter, E., and Muller, R. (1948). "Formulas for bed load transport." Proc., 2nd Meeting IAHR, Stockholm, 39–64.

Nelson, J. M. and Smith, J. D. (1989). "Evaluation and stability of erodible channel beds." River Meandering, AGU, Water Resources Monograph, 12, 321–377.

Nikuradse, J. (1933). "Lows of flow in rough pipes." NACA Tech. Memo.

Rattray, M. Jr. and Mitsuda E.(1974). "Theoretical analysis of conditions in a salt wedge." Estuaric and Coastal Marine Science, 2, 373–394.

Smith, J. D., and McLean, S. R. (1977). "Spatially averaged flow over a wavy surface." J. Geophysical Res., 82, 1735–1746.

Williams, G. P. (1970). "Flume width and water depth effects in sediment–transport experiments." Prof. Paper 562–H, U.S. Geological Survey, Reston, Va.

Yalin, M. S. (1963). "An expression for bed load transportation." J. Hydr. Div. ASCE, 89(HY3), 221–250.

Wiberg, P. L. and Smith, J. D. (1989). "Model for calculating bed load transport of sediment." J. Hydr. Div. ASCE, 115(1), 101–123.

APPENDIX II. – NOTATION

The following symbols are used in this paper

A = cross sectional area;
C_D = form drag coefficient;
D = flow depth;
d = grain sizes;
g = acceleration due to gravity;
H_B = bed form height;
K = kinematic eddy viscosity;
K_0 = value of K at $\int_0^{\ell} dA = 0.2 \int_0^{\ell_m} dA$;
k = Von Karman's constant;
ℓ = distance from boundary along the ray;
ℓ_0 = roughness height at boundary;
ℓ_m = length of ray;
n = cross-stream coordinate;

P_B = perimeter along the boundary;
P_ℓ = perimeter along the isovel;
p = wetted perimeter;
Q = net discharge of flow;
q = discharge per unit width;
q_s = sediment discharge per unit width;
R = ratio of boundary shear stress to that obtained from depth-slope product;
R_* = cross sectional averaged value of the ratio of bed shear stress to the shear stress obtained from the depth-slope product;
S = surface slope of the stream;
u = velocity component in the downstream direction;
u_s = surface velocity;
$< u >$ = vertically averaged value of u;
u_* = shear velocity;
u_{*W} = shear velocity at the wall;
W = channel width;
x = downstream coordinate;
Z_{0B} = roughness height of bed;
Z_{0W} = roughness height of side walls;
$(Z_0)_{SF}$ = roughness length for internal boundary;
z = vertical coordinate;
β = constant, 6.24;
γ = area weighted function of ℓ along the rays;
γ_D = $[(\tau_{SF} + \tau_0)/\tau_{SF}]^{1/2}$;
δ_B = height of saltation layer;
θ = angle of ray to horizontal line;
λ = bed form wave length;
ν = viscosity of water;
ξ = Z/D;
ξ_0 = Z_{0B}/D;
ρ = density of fluid;
ρ_s = density of bed material;
τ_0 = boundary shear stress obtained from depth-slope product;
$(\tau_0)_{AV}$ = the shear stress averaged over the wetted perimeter;
τ_{SF} = skin friction;
τ_B = boundary shear stress;
τ_{CR} = critical shear stress;
τ_* = nondimensional boundary shear stress;
ϕ = nondimensional sediment transport rate;

(Received July 13, 1990; revised November 16, 1990)